Fe/N/C Electrocatalysts for ORR

DOI: 10.1002/ange.201405314

Unravelling the Structure of Electrocatalytically Active Fe–N Complexes in Carbon for the Oxygen Reduction Reaction**

*Yansong Zhu, Bingsen Zhang, Xin Liu, Da-Wei Wang, and Dang Sheng Su**

Abstract: *Non-precious Fe/N co-modified carbon electrocatalysts have attracted great attention due to their high activity and stability in oxygen reduction reaction (ORR). Compared to iron-free N-doped carbon electrocatalysts, Fe/N-modified electrocatalysts show four-electron selectivity with better activity in acid electrolytes. This is believed relevant to the unique Fe–N complexes, however, the Fe–N structure remains unknown. We used o,m,p-phenylenediamine as nitrogen precursors to tailor the Fe–N structures in heterogeneous electrocatalysts which contain FeS and Fe_3C phases. The electrocatalysts have been operated for 5000 cycles with a small 39 mV shift in half-wave potential. By combining advanced electron microscopy and Mössbauer spectroscopy, we have identified the electrocatalytically active Fe–N_6 complexes (FeN_6, [Fe^{III}(porphyrin)(pyridine)$_2$]). We expect the understanding of the FeN_6 structure will pave the way towards new advanced Fe–N based electrocatalysts.*

Fuel cells, as a clean and efficient power source, have attracted significant attention during the last decades.[1] The cathodic oxygen reduction reaction (ORR) is at the heart of fuel cell performance, and efficient ORR electrocatalysts are essential for practical applications. It is critical to replace Pt-based electrocatalysts in order to reduce the manufacturing cost of proton exchange membrane fuel cells (PEMFCs). Non-precious metal catalysts (NPMCs) with high ORR activity and stability have become a major focus of the PEMFC research.[2] At present, NPMCs with high activity and stability in the acid solution are mainly synthesized through pyrolysis of precursors comprising transition metals, nitrogen and carbon (M/N/C).[3] Recent studies on pyrolyzed Fe/N/C and FeCo/N/C catalysts for ORR have reached a high level in both activity[1c] and stability.[4] Since Jasinski reported that a N_4-chelate complex with a non-noble metal core could be used to electrochemically reduce oxygen in 1964,[5] various macrocyclic transition-metal compounds, such as porphyrins, phthalocyanines, and tetraazaannulenes,[6] have been investigated. However, the actual structures of active sites in pyrolyzed M/N/C electrocatalysts remain elusive. Because the M/N/C electrocatalysts are inherently highly heterogeneous and have complex structure, it is very challenging to characterize the right active sites. The active sites in M/N/C ORR electrocatalysts have been often assumed to be M–N_x in acid solution despite the lack of convictive structural determination.[7] Here, we aim to determine the structures of active sites in the Fe/N/C ORR electrocatalysts by using advanced electron microscopy and Mössbauer spectroscopy, and to elucidate the structure–performance relationship in the Fe/N/C electrocatalysts.

We synthesized three Fe/N-containing electrocatalysts by pyrolyzing polymerized *o,m,p*-phenylenediamine, ferric chloride and carbon black. Ammonium peroxydisulfate was added to facilitate phenylenediamine polymerization; this introduced sulfur into the final electrocatalysts. The electrocatalysts are denoted as P*o*PD-Fe-C, P*m*PD-Fe-C, and P*p*PD-Fe-C. The synthesis details are provided in the Supporting Information. The activity and stability of the electrocatalysts were investigated by electrochemical voltammetry in acid solution. X-ray photoelectron spectroscopy (XPS), X-ray diffraction (XRD), electron microscopy, and Mössbauer spectroscopy were conducted to study the structure of active sites in the catalysts. The electrocatalytic characteristics of the active sites and the synthesis–structure–performance relationship were systematically investigated.

The electrocatalytic performance of these three electrocatalysts for ORR in 0.5 M H_2SO_4 were investigated by using linear sweep voltammetry (LSV), as shown in Figure 1 a. The onset potentials for P*o*PD-Fe-C, P*m*PD-Fe-C, and P*p*PD-Fe-C are 0.681, 0.819, and 0.826 V vs. RHE, respectively. Because the onset potential for P*o*PD-Fe-C is far lower than the other two, we consider the active sites in P*m*PD-Fe-C and P*p*PD-Fe-C may have similar structures which are distinct from that in P*o*PD-Fe-C. Note that the kinetic current and the limiting current for P*m*PD-Fe-C are smaller than that for P*p*PD-Fe-C. This may imply the higher quality and density of the active sites in the latter. These distinctions are believed relevant to the diversified microscopic morphologies of the original polymers which could be resulted from the different polymerization chemistry (Figure S1 and S2 in the Supporting Information). Note that P*p*PD has the smallest particle size

[*] Y. S. Zhu, B. S. Zhang, Prof. D. S. Su
Shenyang National Laboratory for Materials Science
Institute of Metal Research, Chinese Academy of Sciences
Shenyang, Liaoning, 110016 (China)
E-mail: dssu@imr.ac.cn
Y. S. Zhu
School of Chemistry and Life Science, Anshan Normal University
Anshan, Liaoning, 114005 (China)
X. Liu
Dalian Institute of Chemical Physics, Chinese Academy of Sciences
Dalian, Liaoning, 116023 (China)
D. W. Wang
School of Chemical Engineering, UNSW Australia
UNSW Sydney, NSW 2052 (Australia)

[**] The authors acknowledge the financial support from MOST (2011CBA00504), NSFC of China (21133010, 21203215, 51221264, 21261160487), and 'Strategic Priority Research Program' of the Chinese Academy of Sciences, Grant No. XDA09030103.

Supporting information for this article is available on the WWW under http://dx.doi.org/10.1002/anie.201405314.

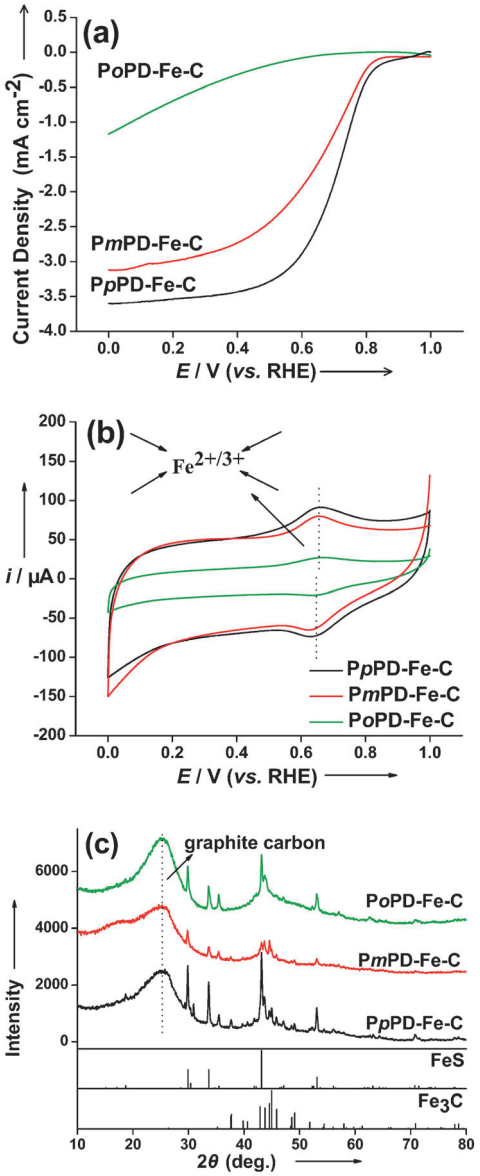

Figure 1. a) RDE voltammograms in O_2-saturated 0.5 M H_2SO_4, scan rate: 5 mV s^{-1}, rotation rate: 900 rpm. b) Cyclic voltammetry in N_2-saturated 0.5 M H_2SO_4, scan rate: 10 mV s^{-1}. c) XRD patterns of P*o*PD-Fe-C, P*m*PD-Fe-C, and P*p*PD-Fe-C. (PDF-FeS: 37-0477; PDF-Fe_3C: 72-1110.)

(≈1 μm), with medium sized P*m*PD particles (2–3 μm) while P*o*PD particles are the largest (10–40 μm), which is consistent with the specific surface area (Table S1). Notably the P*p*PD particles are sheet-like and porous, while P*m*PD particles are spherical with smooth surface. As the thermal pyrolysis is a solid state reaction, smaller size and two-dimensional morphology of N-containing polymer particles may facilitate the diffusion of iron atoms which is critical for forming ORR active Fe–N complexes.

It is believed that N-doped active sites are often accompanied with iron species.[8] In other words, the location and structure of iron species in our heterogeneous Fe/N/S/C electrocatalysts can indicate the actual active sites. Therefore, the content, distribution and structure of the iron in these electrocatalysts are studied in detail combining thermogravimetric analysis, XRD and TEM. As shown in Table S2 and Figure S3, the Fe contents in P*o*PD-Fe-C, P*m*PD-Fe-C, and P*p*PD-Fe-C are 9.88 wt%, 10.92 wt%, and 12.08 wt%, respectively. The higher iron contents in P*m*PD-Fe-C and P*p*PD-Fe-C could be ascribed to the smaller particle size of their polymer precursors which facilitates the iron reaction with carbon, nitrogen and sulfur. It is doubtful that the total Fe contents can be correlated to the ORR activity, because there may be several forms of Fe other than Fe–N complexes in the heterogeneous catalysts. XRD was used to analyze the phase composition in the catalysts (Figure 1c). All three samples show well-developed crystalline structures, assignable mainly to FeS and Fe_3C. Based on the intensities and FWHMs of the diffraction peaks, the particle size and crystallization of iron species are slightly different. In order to confirm whether FeS and Fe_3C are active sites for ORR, the fine structures of FeS and Fe_3C particles were further investigated.

Figure 2a shows a STEM image of P*p*PD-Fe-C. It can be seen that the bright large particles are Fe-containing grains. EDX elemental maps in Figure 2d reveal that the large particles are mainly FeS. The HRTEM image of FeS particles shows that the FeS particle is tightly covered with graphitic carbon and the thickness of the graphitic carbon shell is about 10 nm (Figure 2b). Fe_3C particles are not found in the images

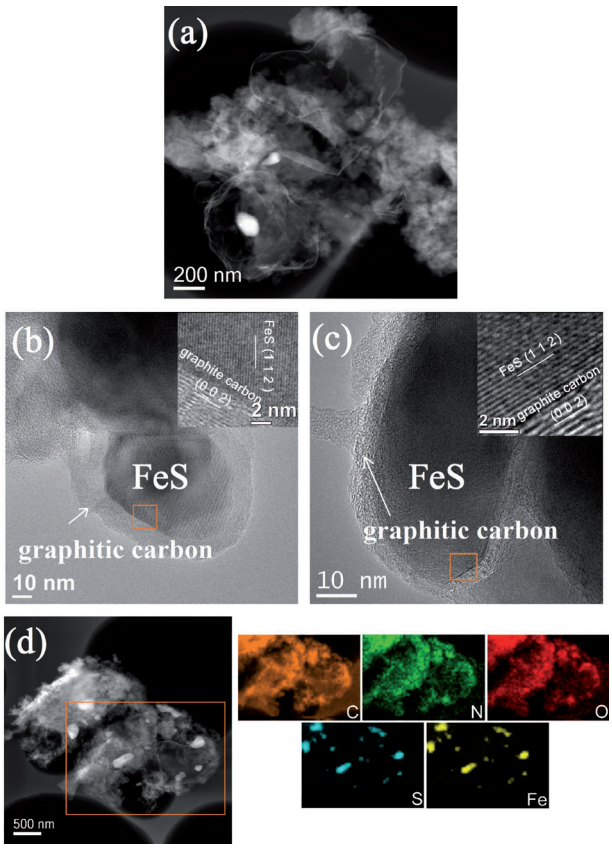

Figure 2. a) STEM image P*p*PD-Fe-C. b) HRTEM image of P*p*PD-Fe-C. c) HRTEM image of P*p*PD-Fe-C after 5000 cycles. d) HAADF-STEM maps of P*p*PD-Fe-C.

of HRTEM. Fe_3C particles may be at the interface of graphitic carbon shell and FeS particles, or covered with graphitic carbon. Otherwise, Fe_3C particles should be removed by acid-leaching because of their poor stability in acid. Figure 2c shows the HRTEM image of FeS particles in P*p*PD-Fe-C that undergoes 5000 cycles in N_2-saturated acid in the potential range from 0.6 to 1.0 V. The shell of covered graphitic carbon is not damaged and is very stable after a long time test, which indicates that FeS covered with graphitic carbon has no chance to catalyze the ORR. Therefore, FeS and Fe_3C covered with graphitic carbons could not be active sites.

The cyclic voltammetry (CV) curves of P*o*PD-Fe-C, P*m*PD-Fe-C, and P*p*PD-Fe-C in Figure 1b show a pair of reversible redox peaks around 0.64 V (the peak separation is 40 mV). We assign this redox reaction to the reduction/oxidation Fe^{3+}/Fe^{2+} in the catalysts (one explanation for the less than 59 mV peak separation is Fe^{3+}/Fe^{2+} exists in the solid catalysts which may allow smaller electron transfer barrier compared to aqueous ions). The reversible redox peaks of Fe^{3+}/Fe^{2+} are always obtained in the CV curve of iron coordination compounds like $[Fe(CN)_6]^{3-}/[Fe(CN)_6]^{4-}$. However, they are impossible to be observed in the CV curve of FeS and Fe_3C, not to mention FeS and Fe_3C covered with graphitic carbon. Since the peak current represents the content of Fe^{3+}/Fe^{2+}, the Fe^{3+}/Fe^{2+} contents in P*p*PD-Fe-C and P*m*PD-Fe-C are higher than that in P*o*PD-Fe-C. We believe the Fe^{3+}/Fe^{2+} content correlates with the ORR activity of the three catalysts. Therefore, in addition to FeS and Fe_3C, there are Fe^{3+}/Fe^{2+} coordination compounds in the catalysts which should distribute on the electrochemical accessible surface of the catalysts. It may be concluded that the iron coordination compounds are real active sites for ORR. The distribution and fine structure of the iron coordination compounds in the electrocatalysts are further investigated. From the STEM image of another area in P*p*PD-Fe-C (Figure 3a), some small bright dots are seen (location marked with red circles). Due to the higher brightness, these dots should be iron containing. But no diffraction spot is found in the selected area electron diffraction pattern (Figure 3b).This indicates that the small particles are not the nanocrystals of either iron, FeS or Fe_3C, but are very fine clusters containing Fe which are very likely Fe–N complexes. As shown in Figure 3c, the distribution of Fe element is uniform in P*p*PD-Fe-C sample except for some big particles. However, the molecular structure of the Fe–N complexes can hardly be determined by electron microscopy.

Fe–N_4 coordination was previously proposed for the electrocatalytic active sites.[9] By using XPS, the nitrogen species in P*o*PD-Fe-C, P*m*PD-Fe-C, and P*p*PD-Fe-C were analyzed, as shown in Figure 4a. N–Fe peaks at a binding energy of 398.9 eV are found in these samples.[2b] The semi-quantitative results of the N group contents are given in Table S3. The quantity of N–Fe bonds in P*o*PD-Fe-C is less than those in P*m*PD-Fe-C and P*p*PD-Fe-C. As mentioned above, the different N–Fe contents can result from the

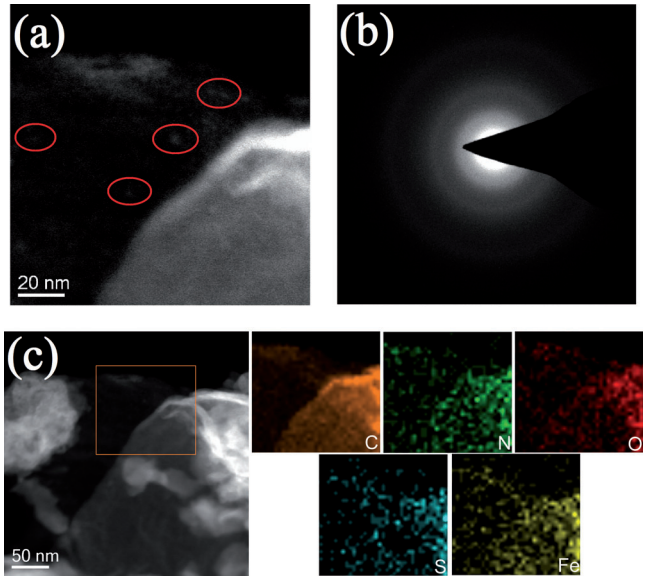

Figure 3. a) STEM image P*p*PD-Fe-C. b) Selected area electron diffraction pattern from the area shown in (a). c) HAADF-STEM maps of P*p*PD-Fe-C.

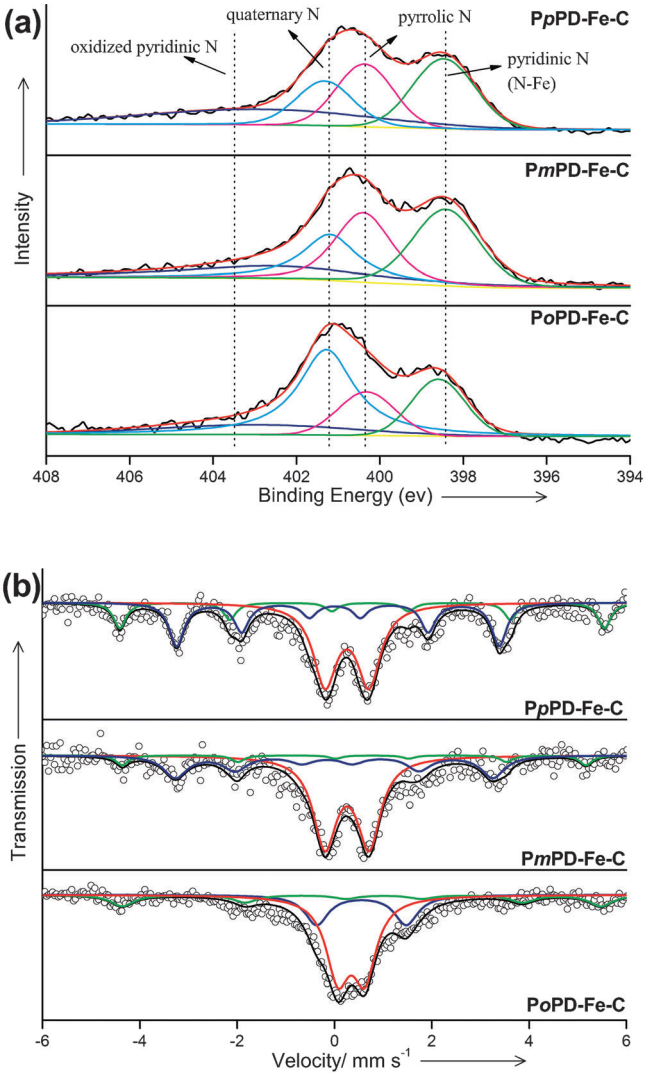

Figure 4. a) N1s XPS spectra of P*o*PD-Fe-C, P*m*PD-Fe-C, and P*p*PD-Fe-C. b) Mössbauer spectra for P*o*PD-Fe-C, P*m*PD-Fe-C, and P*p*PD-Fe-C.

different polymerization and surface states of the polymerized *o*,*m*,*p*-phenylenediamine isomers. It is understood that the quantity of N–Fe bonds may affect the reaction current but does not cause a big difference in the onset potential. It is thus reasonable to speculate that the N–Fe bonds form different coordinated structures in the three electrocatalysts which could be determinant for the activity and onset potential.

Mössbauer spectroscopy is a technique based on the recoil-free absorption of γ rays by Fe^{57} nuclei, and is used to investigate the electron structure of the iron coordination compounds, as shown in Figure 4b. Three kinds of Fe are found in P*o*PD-Fe-C, P*m*PD-Fe-C, and P*p*PD-Fe-C catalysts from the peak fitting. The green curves are unambiguously assigned to FeS. The blue curves with the apparent sextet correspond to Fe_3C.[10] FeS and Fe_3C are also detected by XRD. The most species in the Mössbauer spectra correspond to the red curves with the doublet. From Table S4, the values of isomer shift (IS) of the doublets in three catalysts are 0.454, 0.372, and 0.374 $mm\,s^{-1}$, respectively. So the doublets are assigned to six-coordinate Fe^{III}.[11] The IS values of P*m*PD-Fe-C and P*p*PD-Fe-C (0.372, 0.374 $mm\,s^{-1}$) are very close, and are lower than the value of P*o*PD-Fe-C (0.454 $mm\,s^{-1}$). Since the value of IS becomes larger with increasing ligand bond length, we can predict that the Fe–N bond length is in the order of P*p*PD-Fe-C < P*m*PD-Fe-C < P*o*PD-Fe-C. Taking into account the order of the ORR activity, it is obvious that a shorter Fe–N bond gives rise to higher activity. Considering the poor catalytic activity of P*o*PD-Fe-C, six-coordinate Fe^{III} in P*m*PD-Fe-C and P*p*PD-Fe-C is analyzed in detail. The peak-to-peak separations (quadrupole splitting, QS) are 0.91 and 0.90 $mm\,s^{-1}$ for P*m*PD- Fe-C and P*p*PD-Fe-C, respectively. The values of IS and QS for these two catalysts should be assigned to six-coordinate Fe^{III}, [Fe^{III}(porphyrin)-(pyridine)$_2$] (Scheme 1).[12] Therefore we propose [Fe^{III}(porphyrin)(pyridine)$_2$] as the active sites in our Fe/N/S-modified carbon electrocatalysts for ORR. Note that the six-coordinate FeN_6 complex with tetrapyrrodic N and two pyridinic N may be more durable than FeN_4 in acid solution.

Finally, the integral structure, the electrocatalytic activity and stability, and the kinetic parameters of P*p*PD-Fe-C were studied. As can be seen from Figure S4a and b, both pristine carbon black and carbon black coated with P*p*PD polymer preserve graphitic structure after heat treatment. The graphite structure provides good electrical conductivity so that the electrons can easily reach the active sites. Figure S5a shows the LSV curves of Pt/C (Pt wt% = 20%, in 0.1M $HClO_4$), P*p*PD-C, and P*p*PD-Fe-C. It is found that P*p*PD-C without Fe has no significant limiting current plateau and the onset potential is only 0.4–0.5 V. There is no doubt that the iron plays a decisive role in Fe/N/C catalysts for ORR. Comparing Pt/C (loading of 0.06 $mg_{Pt}\,cm^{-2}$) and P*p*PD-Fe-C, the differences in the half-wave potential ($\Delta E_{1/2}$) and onset potential are 79 mV and 89 mV, respectively. A stability study of P*p*PD-C and P*p*PD-Fe-C catalysts were carried out in a potential range from 0.6 to 1.0 V (rotating disk electrode, RDE) in nitrogen gas at a scan rate of 10 $mV\,s^{-1}$ (Figure S5b). After 5000 RDE cycles, the changes of the half-wave potential for P*p*PD-C and P*p*PD-Fe-C catalysts are 40 mV and 39 mV, respectively. The Koutecky–Levich plots (Figure S5c) are drawn from the ORR curves based on the Koutecky–Levich equation:

$$-\frac{1}{I}=-\frac{1}{I_k}+\frac{1}{0.62nFAD^{2/3}\nu^{-1/6}\omega^{1/2}C_{O_2}} \quad (1)$$

(F=96485 $C\,mol^{-1}$, $A=0.19625\ cm^2$, $D=2.1\times10^{-5}\ cm^2\,s^{-1}$, $C_{O_2}=1.13\times10^{-6}\ mol\,cm^{-3}$, $\nu=9.5\times10^{-3}\ cm^2\,s^{-1}$).[13] Based on the slope of the Koutecky–Levich plots, the number of electrons transferred (the value of n in the overall reaction) is about 3.8. It suggests that the ORR catalyzed by P*p*PD-Fe-C is a four-electron process. From Tafel ORR plot with P*p*PD-Fe-C (Figure S5d), Tafel slope and exchange current density (i_0) for the P*p*PD-Fe-C catalysts are obtained (Table 1). The i_0 value for P*p*PD-Fe-C ($1.5\times10^{-8}\ A\,cm^{-2}$) is lower than for the Pt/C catalyst ($3.2\times10^{-8}\ A\,cm^{-2}$), and the Tafel slope of ORR for P*p*PD-Fe-C (105 $mV\,dec^{-1}$) is higher than that of the Pt/C catalyst (93 $mV\,dec^{-1}$). The higher i_0 value and the lower Tafel slope can both cause the lower onset overpotential (η). In other words, creating the same kinetic current density needs lower overpotential with the higher i_0 value and the lower Tafel slope. Although the performance of the P*p*PD-Fe-C catalyst falls short of Pt/C in terms of half-wave potential and onset potential, i_0 value and Tafel slope of P*p*PD-Fe-C is quite competitive.

In conclusion, we synthesized three Fe/N/S-modified carbon electrocatalysts through heat treatment of polymerized *o*,*m*,*p*-phenylenediamine, ferric chloride, and carbon black. By using advanced electron microscopy and Mössbauer spectroscopy, we confirm that the real active sites for ORR in the catalysts are FeN_6, a Fe^{III} coordination compound with six-coordinate [Fe^{III}(porphyrin)(pyridine)$_2$]. Moreover, we demonstrate high activity and good durability of P*p*PD-Fe-C as a non-precious metal catalyst for ORR. We believe that the knowledge of the real active site FeN_6 will lead the way to target-specific synthesis of highly active and stable Fe/N/C catalysts for ORR.

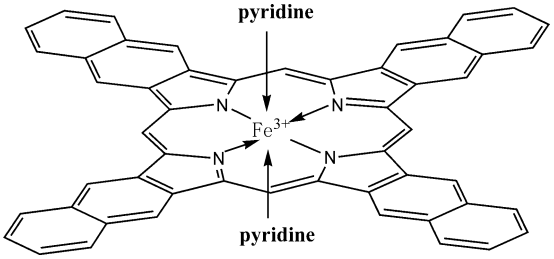

Scheme 1. Possible iron complex structure (adapted from Ref. [12]).

Table 1: ORR kinetics data for P*p*PD-Fe-C catalyst and Pt/C.

Catalyst	Onset potential [V]	$E_{1/2}$ [V]	Tafel slope [$mV\,dec^{-1}$]	i_0 [$A\,cm^{-2}$]
P*p*PD-C	0.498	0.327	205	4.1×10^{-9}
P*p*PD-Fe-C	0.826	0.718	105	1.5×10^{-8}
Pt/C	0.905	0.807	93	3.2×10^{-8}

Received: May 15, 2014
Revised: June 19, 2014
Published online: August 12, 2014

Keywords: active sites · electrocatalysts · iron · Mössbauer spectroscopy · oxygen reduction reaction

[1] a) D. S. Su, G. Sun, *Angew. Chem.* **2011**, *123*, 11774 – 11777; *Angew. Chem. Int. Ed.* **2011**, *50*, 11570 – 11572; b) D.-W. Wang, D. Su, *Energy Environ. Sci.* **2014**, *7*, 576 – 591; c) G. Wu, K. L. More, C. M. Johnston, P. Zelenay, *Science* **2011**, *332*, 443 – 447.

[2] a) F. Jaouen, E. Proietti, M. Lefèvre, R. Chenitz, J.-P. Dodelet, G. Wu, H. T. Chung, C. M. Johnston, P. Zelenay, *Energy Environ. Sci.* **2011**, *4*, 114 – 130; b) G. Wu, C. M. Johnston, N. H. Mack, K. Artyushkova, M. Ferrandon, M. Nelson, J. S. Lezama-Pacheco, S. D. Conradson, K. L. More, D. J. Myers, *J. Mater. Chem.* **2011**, *21*, 11392 – 11405; c) G. Wu, P. Zelenay, *Acc. Chem. Res.* **2013**, *46*, 1878 – 1889.

[3] a) Y. Li, T. Li, M. Yao, S. Liu, *J. Mater. Chem.* **2012**, *22*, 10911 – 10917; b) R. Liu, C. von Malotki, L. Arnold, N. Koshino, H. Higashimura, M. Baumgarten, K. Müllen, *J. Am. Chem. Soc.* **2011**, *133*, 10372 – 10375.

[4] M. Lefèvre, E. Proietti, F. Jaouen, J.-P. Dodelet, *Science* **2009**, *324*, 71 – 74.

[5] R. Jasinski, *Nature* **1964**, *201*, 1212 – 1213.

[6] a) J. Maruyama, J. Okamura, K. Miyazaki, Y. Uchimoto, I. Abe, *J. Phys. Chem. C* **2008**, *112*, 2784 – 2790; b) H. Wang, R. Cote, G. Faubert, D. Guay, J. Dodelet, *J. Phys. Chem. B* **1999**, *103*, 2042 – 2049; c) J. M. Ziegelbauer, T. S. Olson, S. Pylypenko, F. Alamgir, C. Jaye, P. Atanassov, S. Mukerjee, *J. Phys. Chem. C* **2008**, *112*, 8839 – 8849.

[7] a) H. Kalvelage, A. Mecklenburg, U. Kunz, U. Hoffmann, *Chem. Eng. Technol.* **2000**, *23*, 803 – 807; b) M. Lefevre, J. Dodelet, P. Bertrand, *J. Phys. Chem. B* **2000**, *104*, 11238 – 11247; c) M. Lefèvre, J. Dodelet, P. Bertrand, *J. Phys. Chem. B* **2002**, *106*, 8705 – 8713.

[8] Y. Li, W. Zhou, H. Wang, L. Xie, Y. Liang, F. Wei, J.-C. Idrobo, S. J. Pennycook, H. Dai, *Nat. Nanotechnol.* **2012**, *7*, 394 – 400.

[9] a) J. Blomquist, U. Helgeson, L. Moberg, L. Johansson, R. Larsson, *Electrochim. Acta* **1982**, *27*, 1445 – 1451; b) S. L. Gojković, S. Gupta, R. Savinell, *J. Electroanal. Chem.* **1999**, *462*, 63 – 72; c) S. Gupta, D. Tryk, S. Zecevic, W. Aldred, D. Guo, R. Savinell, *J. Appl. Electrochem.* **1998**, *28*, 673 – 682; d) J. R. Van Veen, J. F. van Baar, K. J. Kroese, *J. Chem. Soc.* **1981**, *77*, 2827 – 2843.

[10] a) C. R. Johnson, R. E. Shepherd, *Inorg. Chem.* **1983**, *22*, 3506 – 3513; b) D. Sedney, M. Kahjehnassiri, W. M. Reiff, *Inorg. Chem.* **1981**, *20*, 3476 – 3481; c) J. Tian, A. Morozan, M. T. Sougrati, M. Lefèvre, R. Chenitz, J. P. Dodelet, D. Jones, F. Jaouen, *Angew. Chem.* **2013**, *125*, 7005 – 7008; *Angew. Chem. Int. Ed.* **2013**, *52*, 6867 – 6870.

[11] U. I. Koslowski, I. Abs-Wurmbach, S. Fiechter, P. Bogdanoff, *J. Phys. Chem. C* **2008**, *112*, 15356 – 15366.

[12] M. H. M. Rein, *Chem. Ber.* **1988**, *121*, 1601 – 1608.

[13] a) S. Baranton, C. Coutanceau, E. Garnier, J.-M. Léger, *J. Electroanal. Chem.* **2006**, *590*, 100 – 110; b) K.-L. Hsueh, D.-T. Chin, S. Srinivasan, *J. Electroanal. Chem. Inter. Electrochem.* **1983**, *153*, 79 – 95; c) R. N. Itoe, G. Wesson, E. E. Kalu, *J. Electrochem. Soc.* **2000**, *147*, 2445 – 2450; d) D. R. Lawson, L. D. Whiteley, C. R. Martin, M. N. Szentirmay, J. I. Song, *J. Electrochem. Soc.* **1988**, *135*, 2247 – 2253.

